Langmuir

Article

pubs.acs.org/Langmuir

Photoreduction of 4,4′-Dimercaptoazobenzene on Ag Revealed by Raman Scattering Spectroscopy

Kwan Kim,*[,†] Kyung Lock Kim,[†] and Kuan Soo Shin*[,‡]

[†]Department of Chemistry, Seoul National University, Seoul 151-742, Korea

[‡]Department of Chemistry, Soongsil University, Seoul 156-743, Korea

Supporting Information

ABSTRACT: The surface-enhanced Raman scattering (SERS) of 4,4′-dimercaptoazobenzene (4,4′-DMAB) has recently seen a surge of interest, since it might be possible to form 4,4′-DMAB from 4-aminobenzenethiol (4-ABT) via a surface-induced photoreaction. We found in this study, however, that the reverse conversion of 4,4′-DMAB to 4-ABT on Ag is a more feasible process upon irradiation with a 514.5 nm (not 632.8 nm) laser under ambient conditions. First of all, the SERS spectral pattern of 4,4′-DMAB on Ag varied as a function of laser irradiation time, finally becoming the same as that of 4-ABT on Ag. Second, the coupling reaction with 4-cyanobenzoic acid to form amide bonds proceeded readily like 4-ABT once 4,4′-DMAB on Ag was exposed to 514.5 nm radiation. Third, the growth of a calcite crystal occurred on 4,4′-DMAB on Ag, also likely on 4-ABT, when it was exposed to 514.5 nm radiation beforehand. All of these results led us to conclude that the appearance of the so-called b_2-type bands in the SERS of 4-ABT must be due to the involvement of the chemical enhancement mechanism, not due to the formation of 4,4′-DMAB.

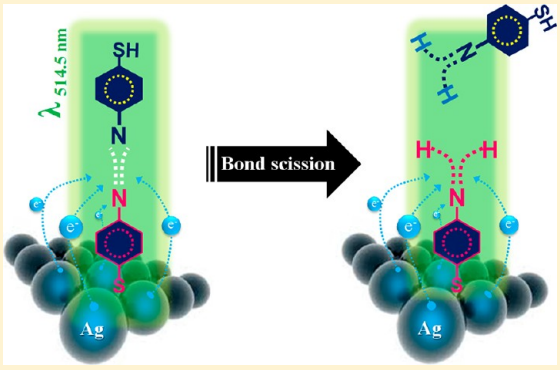

1. INTRODUCTION

Surface-enhanced Raman scattering (SERS) is a surface-sensitive technique that enhances Raman scattering by molecules on rough metal surfaces, especially gold and silver.[1] In particular, the enhancement factor can be as much as 10^{14}–10^{15} for dye molecules including the contribution of the resonance Raman scattering, which means that the technique may detect single molecules.[2−5] There are two primary theories that can account for the signal enhancement, one being the electromagnetic field enhancement theory and the other being the chemical enhancement theory. The electromagnetic theory is based on the excitation of localized surface plasmons, while the chemical theory assumes the formation of charge-transfer complexes.[6,7] The electromagnetic theory can apply even in cases when the molecules are physisorbed onto the SERS-active substrate, while the chemical theory is applicable only to cases in which the molecules have formed a chemical bond with the SERS substrate.[1−7] In any case, both mechanisms suggest the possibility of enhanced absorption and photochemistry for surface-adsorbed molecules, although experimentally distinguishing the contributions of each mechanism is not so straightforward. The direct observation of a surface-enhanced photochemical reaction has indeed been reported.[8−15]

The compound 4,4′-dimercaptoazobenzene (4,4′-DMAB) has recently come to our attention because its SERS spectral features are remarkably similar to those of 4-aminobenzenethiol (4-ABT), especially in Ag nanoaggregates.[16−21] In fact, 4-ABT itself is an unusual molecule in the sense that its SERS spectral features are dependent not only on the nature of the SERS substrate but also on the measurement conditions.[22−28] In the normal Raman (NR) spectrum, only peaks assignable to totally symmetric (a_1) vibrations are observed, but in the SERS spectrum, non-a_1-type peaks are also identified.[16−40] The origin of these additional bands is not certain. One claim is that the bands are the b_2-type bands of 4-ABT arising from the charge-transfer chemical enhancement mechanism.[29] We recently reported that the appearance of the b_2-type bands is a general phenomenon in the SERS of 4-ABT analogues, possibly including 4,4′-DMAB.[38−40] On the other hand, another claim is that the b_2-type bands appearing in the SERS of 4-ABT must be the N═N stretching vibrations of 4,4′-DMAB produced from 4-ABT via a catalytic coupling reaction on the metal substrates.[16−21] The basis for this claim is the spectral similarity of 4-ABT and 4,4′-DMAB. However, only limited data are available on 4,4′-DMAB, which hinders exploration of the origin of the spectral similarity, since 4,4′-DMAB has to be custom synthesized.

We recently investigated the SERS of 4,4′-DMAB trapped in Au nanogaps.[39] First, 4,4′-DMAB is probably adsorbed on a flame-annealed Au substrate via one of its two thiol groups, such that Au nanoparticles can be further adsorbed on the pendent thiol group, forming a SERS hot site. The most

Received: August 19, 2012
Revised: December 1, 2012
Published: December 19, 2012

distinctive feature in the SERS of 4,4′-DMAB was the appearance of a_g bands, which were quite similar to the b_2-type bands occurring in the SERS of 4-ABT. In an electrochemical environment, the a_g bands of 4,4′-DMAB at 1431, 1387, and 1138 cm^{-1} become weaker at lower potentials, completely disappearing at −1.0 V versus a saturated Ag/AgCl electrode.[17] However, the bands were restored when the electrode potential was increased, implying that neither an electro- nor photochemical reaction took place to break the azo group, which agrees with cyclic voltammetry data.[39] Thus, it was concluded that the appearance and disappearance of these a_g bands were associated with the charge-transfer phenomenon.

To clarify the origin of the b_2-type bands of 4-ABT, we recently further examined the similarity and dissimilarity of the SERS spectra of 4-ABT and 4,4′-DMAB, along with the SERS spectrum of the analogous molecule 4,4′-dimercaptohydrazobenzene (4,4′-DMHAB).[40] In fact, under ambient conditions, the SERS spectra of 4-ABT, 4,4′-DMAB, and 4,4′-DMHAB on Ag were comparable to one another, although the excitation wavelength dependence of the peak intensities indicated that the similarity of the SERS spectral patterns was not necessarily the result of photoconversion of the three molecules. On the other hand, spectral dissimilarity was observed not only in the potential-dependent SERS spectra but also in the SERS spectra taken after treating the substrates with a borohydride solution. It appeared that 4,4′-DMAB on Ag could be converted to 4-ABT either by lowering the potential below −1.0 V or by treatment with 100 mM borohydride. Conversely, however, an electrochemical reaction did not take place for 4-ABT or 4,4′-DMHAB on Ag when the electrode potential was lowered even to −1.0 V or when the substrates were treated with a 100 mM borohydride solution.[40] These observations support our previous proposition that the b_2-type bands appearing in the SERS of 4-ABT must be attributable to the chemical enhancement of 4-ABT itself.

In this study, we would like to report that 4,4′-DMAB on Ag can be converted to 4-ABT even photochemically. For that purpose, we carefully examined the spectral variation of 4,4′-DMAB and 4-ABT on Ag as a function of laser irradiation time. When 514.5 nm radiation (with 2.1 mW power at the sampling position) was used as the excitation source, the SERS spectral pattern of 4,4′-DMAB varied gradually for 2 h under ambient conditions, finally becoming the same as that of 4-ABT on Ag. Supposing that the observed spectral variation is suggestive of the photoconversion of 4,4′-DMAB to 4-ABT, we attempted to conduct two different reactions after exposure of 4,4′-DMAB on Ag to 514.5 nm radiation: a 1-ethyl-3-(3-(dimethylamino)-propyl)carbodiimide (EDC)-mediated coupling reaction with 4-cyanobenzoic acid (4-CBA)[41−43] and the biomimetic growth of a calcite crystal.[43−46] Although the EDC coupling reaction did not take place for neat 4,4′-DMAB on Ag, it did proceed after exposure to 514.5 nm radiation, as evidenced by the appearance of the CN stretching band of 4-CBA. As for the crystal growth, micrometer-sized calcite crystals readily grew after laser exposure, although only nanometer-sized calcite crystals were formed in the neat state, supporting the proposed photoconversion of 4,4′-DMAB to 4-ABT on Ag. The present observation completely contradicts claims made by a number of researchers that 4-ABT on Ag is converted photochemically to 4,4′-DMAB, not the reverse one.

2. EXPERIMENTAL SECTION

2.1. Chemicals and Materials. Silver foil (0.025 mm thick, 99.9%), silver nitrate ($AgNO_3$, 99.99%), sodium citrate (99.9%), 4-ABT (97%), benzenethiol (BT, ≥98%), 3-aminopropyltrimethoxysilane (3-APS, 99%), calcium chloride ($CaCl_2$, 96%), ammonium carbonate ($(NH_4)_2CO_3$, 99.99+%), and EDC (≥98.0%) were purchased from Aldrich, while 4-CBA (98%) and *N*,*N*-dimethylformamide (DMF) (99.0%) were purchased from TCI Co., Ltd., and Samchun Chemical Co., respectively. The compound 4,4′-DMAB (MW = 246.4) was custom synthesized by Medigen Co. and delivered as a light-yellow solid. The parent mass peak (m/z) corresponding to the protonated form of the compound was identified at 247.3 ($[M + H]^+$), and three different protons were identified in the proton NMR spectrum at 3.6 ppm for SH, 7.4 ppm for 2-CH, and 7.8 ppm for 3-CH. Other chemicals, unless specified, were reagent grade, and triply distilled water of resistivity greater than 18.0 MΩ·cm was used throughout the study.

2.2. Preparation of SERS-Active Ag Substrate. Aqueous Ag sol was prepared according to the procedure of Lee and Meisel.[47] Initially, $AgNO_3$ (45 mg) was dissolved in water (250 mL), and the solution was brought to a boil. A solution of 1% sodium citrate (5 mL) was added to the $AgNO_3$ solution under vigorous stirring, and boiling was continued for 1 h. The Ag sol thus prepared was stable for several months at room temperature. Ag nanoparticle films were prepared by dropping the above Ag sol onto glass slide or Si wafer substrates.[48] Initially, the slide glass or Si wafer substrates were subjected to ozonolysis to render them hydrophilic, with a water contact angle of <5°. They were subsequently reacted with 3-APS, following the protocol given in the literature, in order to install amine terminated functionalities.[48] A Viton O-ring with an inner diameter of 5 mm was subsequently placed on the 3-APS-modified slide glass or Si wafer substrate, and then 15 mL of Ag sol was injected inside the O-ring. The injected substrate was left to dry under ambient conditions in order to form a uniform and circular nanoparticle film. After they were washed with deionized water, these Ag films were soaked in a 3 mM ethanolic solution of 4-ABT or 4,4′-DMAB for ∼5 h and then washed with ethanol.

2.3. EDC Coupling and Crystal Growth Methods. To fabricate SERS-active glass capillaries, the inside surfaces of the glass capillaries were first reacted with 3-APS, and then the Ag sol was injected into the capillaries using a syringe. The capillaries were left in that state for 12 h, then the unbound Ag colloids were sucked out using a syringe.[40] Subsequently, ethanolic solutions of 4-ABT or 4,4′-DMAB (2 mM) were injected into the capillaries. After 5 h, the capillaries were washed with ethanol and air-dried. These capillaries were subjected to Raman spectral analyses in the presence of an EDC coupling reagent composed of 0.02 M 4-CBA and 0.02 M EDC in DMF. We also prepared the SERS-active silver substrate by immersing an Ag foil in dilute (1:1) HNO_3 to demonstrate the growth of a crystal. The crystallization of calcium carbonate was conducted by soaking the laser-irradiated sample in a 10 mM $NaHCO_3$ aqueous solution (10 mL) for 10 h, followed by addition of a 10 mM $CaCl_2$ solution (10 mL).

2.4. Characterization Methods. UV−vis spectra were obtained with a SCINCO S-4100 spectrophotometer. The FE-SEM images were obtained with a JEOL JSM-6330F field emission electron microscope operating at 5 kV. Raman spectra were obtained using a Renishaw Raman system Model 2000 spectrometer equipped with an integral microscope (Olympus BH2-UMA). The 514.5 nm line from a 20 mW Ar^+ laser (Melles Griot Model 351MA520) or the 632.8 nm line from a 17 mW He/Ne laser (Spectra-Physics Model 127) were used as the excitation sources, and the Raman scattering was detected over a 180° range with a Peltier-cooled (−70 °C) charge-coupled device (CCD) camera (400 × 600 pixels). The laser beam was focused onto a spot ∼1 μm in diameter, and the laser power at the sampling position was 2.1 and 1.1 mW for the 514.5 and 632.8 nm line, respectively. The Raman band of a silicon wafer at 520 cm^{-1} was used to calibrate the spectrometer, and the accuracy of the spectral measurement was estimated to be better than 1 cm^{-1}.

3. RESULTS AND DISCUSSION

Silver was used in this work as the SERS substrate since 4-ABT on Ag is known to exhibit a SERS spectrum similar to that of 4,4′-DMAB, especially when excited with a 514.5 nm laser. The Ag substrate prepared using citrate-reduced Ag nanoparticles is further known to be SERS active, not only with 514.5 nm radiation but also 632.8 nm radiation, allowing for investigation of the excitation wavelength dependence.[15,40] Figure 1a shows

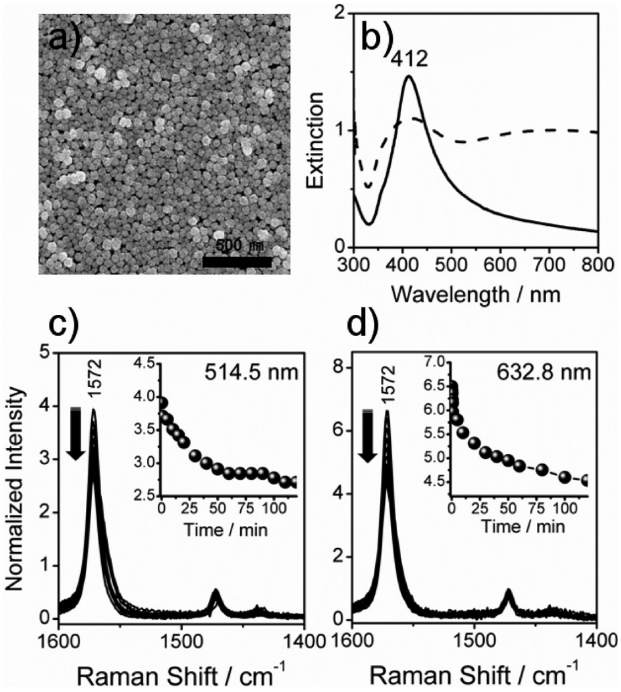

Figure 1. (a) FE-SEM image of Ag nanoparticle film. (b) UV−vis extinction spectra of Ag nanoparticles in the colloidal state (solid line) and film state (dashed line). SERS spectra of BT on Ag nanoparticle film measured using (c) 514.5 nm and (d) 632.8 nm radiation as the excitation source. Insets show the variation of the SERS peak intensity as a function of laser irradiation time.

the field emission scanning electron microscopy (FE-SEM) image of the Ag nanoparticle film assembled on an amine-modified glass substrate. The Ag nanoparticles themselves are faceted and spherical in shape, with a mean diameter of 55 ± 16 nm. Isolated Ag nanoparticles exhibit a surface plasmon resonance (SPR) absorption band at 412 nm, but as they assemble into a close-packed aggregate, the SPR band is broadened into the visible and near-infrared region, as can be seen in Figure 1b. According to the electromagnetic enhancement mechanism, the Ag nanoparticle film must then be highly SERS active not only upon excitation at 514.5 nm but also upon excitation at 632.8 nm. This was tested using BT as the probe molecule. Figures 1c and 1d show the SERS spectra of BT adsorbed on the Ag film measured using 514.5 and 632.8 nm radiation as the excitation source, respectively. Indeed, very intense SERS spectra were obtained at both excitation wavelengths. For later reference, we monitored the variation of the peak intensities of BT at 1572 cm^{-1} for 2 h, which might occur owing to a local heating of the Ag substrate. As shown in the insets of Figures 1c and 1d, the SERS activity of Ag was lowered by about 37% after laser irradiation (not only at 514.5 nm but also at 632.8 nm) for 2 h.

Figures 2a and 2b show the normal Raman (NR) spectra of 4-ABT in the neat state measured using 514.5 and 632.8 nm

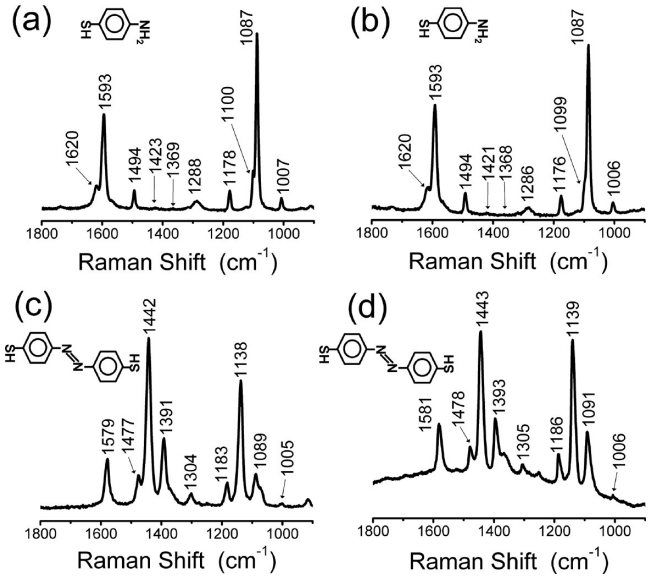

Figure 2. NR spectra of 4-ABT in the neat state measured using (a) 514.5 nm and (b) 632.8 nm radiation as the excitation source. NR spectra of 4,4′-DMAB in the neat state measured using (c) 514.5 nm and (d) 632.8 nm radiation as the excitation source.

radiation as the excitation source, respectively. Similarly, Figures 2c and 2d show the NR spectra of 4,4′-DMAB measured with excitation at 514.5 and 632.8 nm, respectively. For both 4-ABT and 4,4′-DMAB, the NR spectral patterns were insensitive to the excitation wavelength. It is well-known that the spectral region between 1100 and 1500 cm^{-1} is almost featureless in the NR spectrum of 4-ABT, ignoring the very weak peaks at 1178 (ν_{9a}, a_1), 1288 ($\nu_{7a'}$, a_1), and 1494 cm^{-1} (ν_{19a}, a_1).[29] The most intense NR peak for 4-ABT is at 1087 cm^{-1}, which can be attributed to the a_1-type 7a band. In contrast, very intense peaks are identified in the region between 1100 and 1500 cm^{-1} in the NR spectrum of 4,4′-DMAB. These bands, including the band at 1442 cm^{-1}, can be attributed at least partly to the stretching motion of the N═N bond.[16−20] An a_g-type band of 4,4′-DMAB that can be correlated with the 7a band of 4-ABT appears at ∼1090 cm^{-1}, but its intensity is several times lower than that of the N═N stretching band at 1442 cm^{-1}. Here, it is clear that the NR spectral pattern of 4,4′-DMAB is very different from that of 4-ABT.

We subsequently recorded the SERS spectra of 4,4′-DMAB and 4-ABT on the Ag film using 514.5 nm radiation as the excitation source. The peak intensities were normalized with respect to that of a silicon wafer at 520 cm^{-1}. Major peaks in the NR and SERS spectra of 4,4′-DMAB and 4-ABT are collectively summarized in Table S1 of the Supporting Information along with their vibrational assignments; the vibrational assignments of 4,4′-DMAB are taken from the works reported by Fang et al.[16] and Huang et al.,[17] while those of 4-ABT are from the work by Osawa et al.[29] We noticed that the SERS peaks of 4-ABT and 4,4′-DMAB varied as a function of laser irradiation time, as collectively shown in Figures 3a and 3b, respectively. We mentioned above that the SERS peaks of BT on Ag were lowered by as much as 37% after laser irradiation for 2 h, but the spectral pattern itself was maintained. However, in the cases of 4-ABT and 4,4′-DMAB,

dx.doi.org/10.1021/la304159c | Langmuir 2013, 29, 183−190

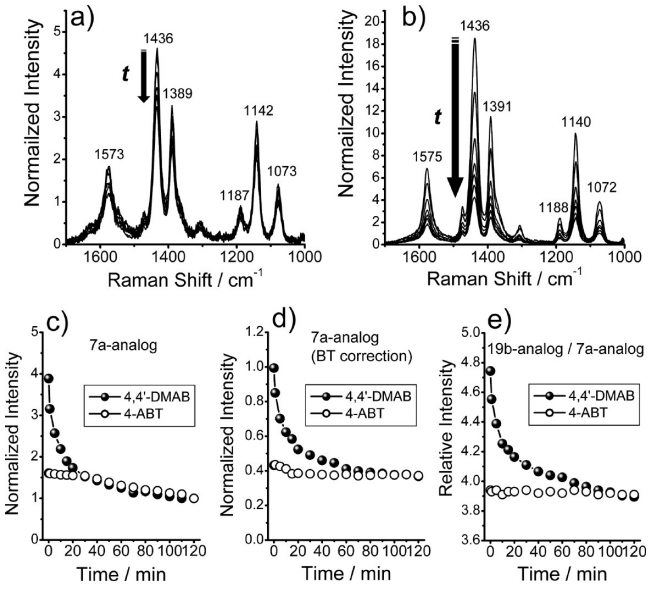

Figure 3. SERS spectra of (a) 4-ABT and (b) 4,4′-DMAB on Ag nanoparticle film measured using 514.5 nm radiation as the excitation source. Spectra measured over time are shown by different lines. (c) Normalized peak intensities of 7a-analogue bands in (a) (empty circles) and (b) (filled circles) shown versus laser irradiation time. (d) The data shown in (c) corrected for the degradation of the SERS activity of the Ag film by referring to the SERS data of BT in Figure 1c. (e) Relative intensity of the 19b- to 7a-analogue bands in (a) and (b) shown versus laser irradiation time.

the SERS spectral patterns themselves were found to vary upon laser irradiation. At any rate, it is evident that the SERS spectral pattern of 4-ABT in Figure 3a is completely different from its NR spectral pattern shown in Figure 2a. In contrast, the SERS spectral pattern of 4,4′-DMAB in Figure 3b is comparable to the NR spectral pattern of 4,4′-DMAB in Figure 2c. Conversely, the SERS spectral pattern of 4,4′-DMAB is surprisingly similar to that of 4-ABT. It is for this reason that a few researchers have claimed that 4-ABT on Ag must have been converted to 4,4′-DMAB by a photoinduced coupling reaction.[16−19] However, we previously claimed that the appearance of new bands in the region of 1100−1500 cm^{-1} in the SERS of 4-ABT were not caused by any surface-induced photoreaction but instead had to do with a phenomenon common to all 4-ABT derivatives, possibly including 4,4′-DMAB, which is associated with the chemical enhancement mechanism in SERS.[38−40]

To support our earlier proposition,[38−40] we carefully monitored the intensity variation of the SERS peaks of 4-ABT and 4,4′-DMAB as a function of laser irradiation time. Assuming that 4-ABT on Ag is not subjected to any photoreaction, the peaks appearing at 1435, 1388, and 1141 cm^{-1} in the SERS of 4-ABT in Figure 3a must be assigned to the b_2-type 19b, 3, and 9b modes, respectively, while the peak at 1090 cm^{-1} is the a_1-type 7a band. For easy comparison of the SERS spectra of 4,4′-DMAB and 4-ABT, we further presume (momentarily) that the SERS peaks of 4,4′-DMAB appearing at similar positions are of the same types as those of 4-ABT. On this basis, the variation of the intensity of the 7a-analogue band at 1090 cm^{-1} in Figure 3b is plotted in Figure 3c as a function of laser irradiation time, along with a similar plot for the 7a band in Figure 3a. The intensity of the 7a-analogue band due to 4,4′-DMAB decreases rapidly for the first 20 min and then slowly as a function of laser irradiation time, while the 7a band of 4-ABT decreases monotonously from the beginning. The decrease in the intensity of the 7a-analogue band at longer irradiation times in Figure 3c must be attributed, at least partly, to the degradation of the Ag film, as seen from the SERS of BT in Figure 1c.[9,49] Shown in Figure 3d is the intensity variation of the 7a-analogue bands after correction for the degradation of the Ag film (deduced from the SERS of BT). It is clear from the figure that the 7a-analogue band from 4,4′-DMAB decreased in intensity by a noticeable amount after laser irradiation, while the 7a band of 4-ABT is affected only by a limited amount. This may indicate that 4,4′-DMAB rather than 4-ABT is subjected to a photoreaction. To closely examine this possibility, we calculated the relative intensity of the 19b-analogue band with respect to the 7a-analogue band and examined its variation relative to the laser irradiation time.

Figure 3e shows the variation of the intensity ratios of the 19b-analogue bands to the 7a-analogue bands in Figures 3a,b. While the intensity ratio for 4-ABT as a function of laser irradiation time remained nearly constant, the intensity ratio observed for 4,4′-DMAB decreased rapidly until it reached the same ratio as that for 4-ABT. Supposing that all of the SERS peaks of 4,4′-DMAB occur without any photoreaction, but by the electromagnetic enhancement mechanism alone, the intensity ratio in Figure 3e must remain constant over time. However, the intensity ratio is found to decrease by as much as 62% over 2 h and then becomes the same as that of 4-ABT. This may suggest that 4,4′-DMAB is converted to 4-ABT by a surface-induced photoreaction. This process is actually opposite to that previously reported by several researchers.[16−20] If the conversion of 4,4′-DMAB to 4-ABT occurs, it must be via a reductive reaction. We recently observed that 4,4′-DMAB on Ag could be reduced to 4-ABT upon treatment with a borohydride solution as well as by lowering potential to −1.2 V versus a saturated Ag/AgCl electrode.[40]

We suppose that 4,4′-DMAB on Ag can be reduced to 4-ABT solely by a surface-induced photoreaction, similar to 4-nitrobenzenethiol on Ag.[43,50,51] To verify the occurrence of such a photoreaction, we attempted an EDC coupling reaction[43] with 4-CBA to form amide bonds after the irradiation of 4,4′-DMAB on Ag with 514.5 nm light. We first confirmed that 4-ABT on Ag reacts readily with 4-CBA in DMF. This is evident from Figure 4b, which shows the SERS spectrum measured after the reaction. For comparison, the SERS spectra of neat 4-ABT and 4,4′-DMAB on Ag are reproduced in Figure 4a. The peak at 2231 cm^{-1} in Figure 4b is due to the CN stretching vibration arising from the formation of amide bonds between the amine group of 4-ABT and the acid group of 4-CBA. The bands at 1661 and 1528 cm^{-1} can be attributed to the amide I and II bands, respectively.[52,53] In contrast, we observed that the as-prepared 4,4′-DMAB on Ag did not react with 4-CBA, as can be seen in Figure 4c (which is hardly different from that in Figure 4a), while the laser-irradiated 4,4′-DMAB on Ag readily reacted with 4-CBA to form amide bonds (even though the reaction was unlikely to produce a 100% yield). This is evident from Figure 4d, which shows the SERS spectrum of 4,4′-DMAB on Ag measured after EDC coupling with 4-CBA following 514.5 nm laser irradiation for 2.5 h. As seen for 4-ABT, we attribute the newly observable peaks at 2230 and 1662 cm^{-1} in Figure 4d to the CN stretching and the amide I band arising from the formation of the amide bond, respectively.[43] This observation strongly supports our

dx.doi.org/10.1021/la304159c | Langmuir 2013, 29, 183−190

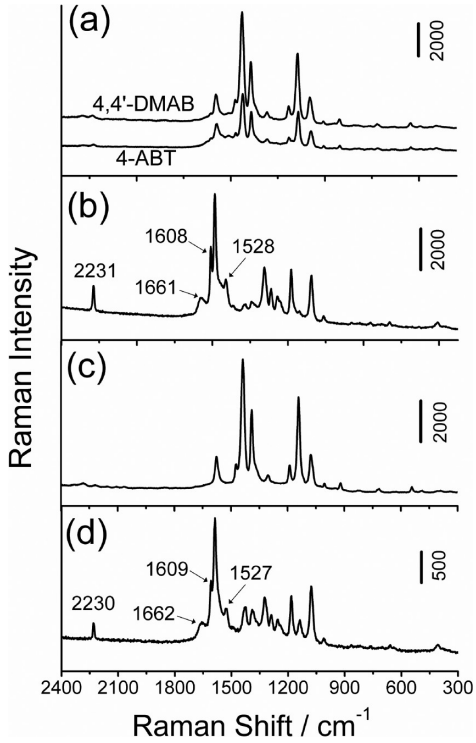

Figure 4. (a) SERS spectra of 4-ABT and 4,4-DMAB on Ag measured before an EDC coupling reaction with 4-CBA. (b) SERS spectrum of 4-ABT on Ag measured after an EDC coupling reaction with 4-CBA. The EDC coupling reaction was performed for 30 min by injecting 0.02 M 4-CBA in DMF containing 0.02 M EDC into a glass capillary coated with 4-ABT-adsorbed Ag nanoparticle film. SERS spectra of 4,4′-DMAB on Ag measured after EDC coupling (c) without irradiation and (d) following 514.5 nm laser irradiation for 2.5 h.

proposition that 4,4′-DMAB on Ag can be converted to 4-ABT by surface-induced photoreduction.

The photoconversion of 4,4′-DMAB upon 514.5 nm radiation was further confirmed by the selective growth of calcium carbonate. It is well-known that functionalized organic surfaces can promote the nucleation of inorganic crystals such as calcite.[43−46] We observed earlier that the crystallization of calcite occurs very facilely on the amine-terminated regions, especially when carbonate ions are allowed to react with the amine groups before a calcium chloride solution is added. In fact, calcite grew readily on 4-ABT on Ag irrespective of the irradiation of either 514.5 or 632.8 nm radiation, while it grew on 4,4′-DMAB on Ag only after the irradiation of 514.5 nm radiation beforehand (see Figure S1). For clarity, after 4,4′-DMAB was self-assembled on Ag, different locations, each with one, two, three, or four spots, were irradiated with a focused Ar^+ laser, and then calcite crystals were grown on the spots after exposing the whole substrate to carbonate ions. As shown in Figure 5, the crystals grew to sizes of ∼15 μm at specific sites, supposedly those exposed to the laser beam to produce the amine functionalities. The identity of calcite was confirmed from its Raman spectrum, as shown in the inset of Figure 5 (1 spot sample).[46] At most, the sizes of the calcite crystals grown on the intrinsic surface of 4,4′-DMAB were as large as 10−20 nm. On the other hand, the growth of a calcite crystal was not observed on 4,4′-DMAB on Ag when it was exposed to 632.8 nm radiation beforehand (*vide infra*).

We separately examined the excitation wavelength dependence. Figures 6a and 6b show a series of SERS spectra of 4-ABT

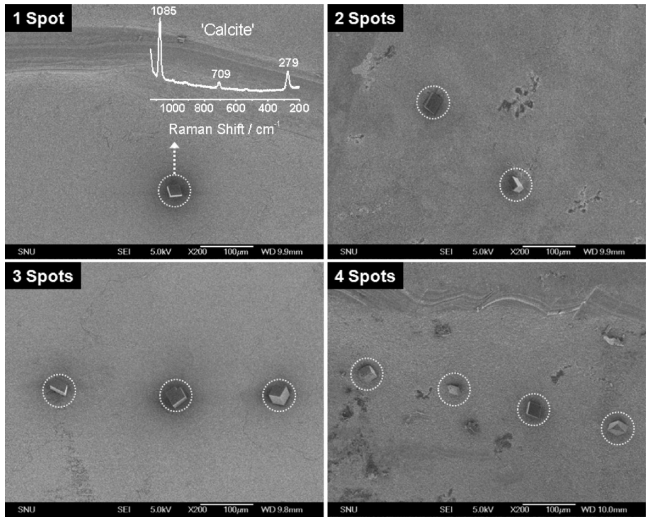

Figure 5. FE-SEM images of calcite crystals grown on 4,4′-DMAB on roughened Ag foil after irradiation with a 514.5 nm laser beforehand at different locations, each with either one, two, three, or four spots. Inset shows the Raman spectrum of the grown calcite.

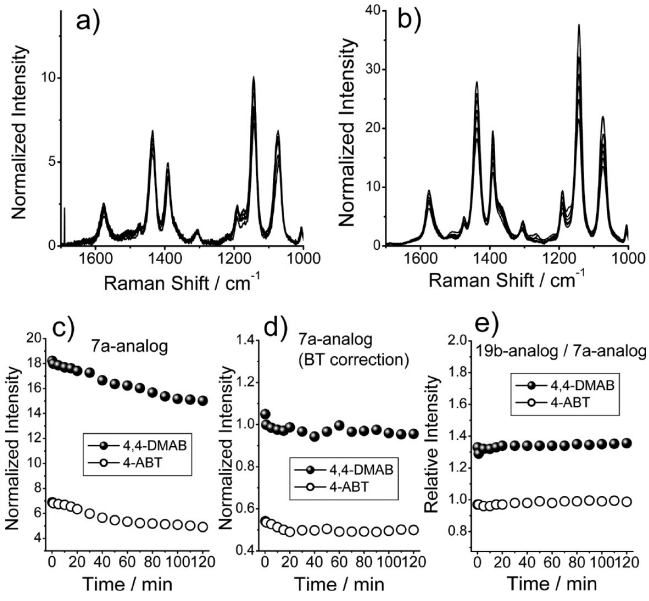

Figure 6. SERS spectra of (a) 4-ABT and (b) 4,4′-DMAB on Ag nanoparticle film measured using 632.8 nm radiation as the excitation source. Spectra measured over time are shown by different lines. (c) Normalized peak intensities of 7a-analogue bands in (a) (empty circles) and (b) (filled circles) shown versus laser irradiation time. (d) The data shown in (c) corrected for the degradation of the SERS activity of the Ag film by referring to the SERS data of BT in Figure 1d. (e) Relative intensity of the 19b- to 7a-analogue bands in (a) and (b) shown versus laser irradiation time.

and 4,4′-DMAB on Ag, respectively, measured as a function of time using 632.8 nm radiation as the excitation source. The measured intensities changed, but their variation was not the same as that observed for irradiation with 514.5 nm light. Figure 6c shows the variation of the intensity of the 7a-analogue band at 1090 cm^{-1} as a function of laser irradiation time. Correcting for the effect of the degradation of the Ag film by referring to the SERS of BT in Figure 1d, the 7a-analogue band intensities remained at a fairly constant level throughout, without merging together, as can be seen in Figure 6d. A similar

dx.doi.org/10.1021/la304159c | *Langmuir* 2013, 29, 183−190

trend is seen for the intensity of the 19b-analogue band relative to that of the 7a-analogue band shown in Figure 6e. That is, the relative intensities also remained fairly constant for both 4,4′-DMAB and 4-ABT. All of these observations suggest that no photoreaction takes place from 4,4′-DMAB to 4-ABT or from 4-ABT to 4,4′-DMAB upon irradiation at 632.8 nm (*vide supra*).

Two particular questions are now raised: namely, how does the conversion of 4,4′-DMAB to 4-ABT on Ag proceed under 514.5 nm irradiation, and what is the hydrogen source? The detailed mechanism of the azo-to-amine conversion on Ag is a matter of conjecture, but photoelectrons are known to be ejected from Ag even upon irradiation by a visible laser: Scheme 1 shows the schematic representation of the photo-

Scheme 1. Schematic Representation of the Photoreduction of 4,4′-DMAB on Ag to 4-ABT

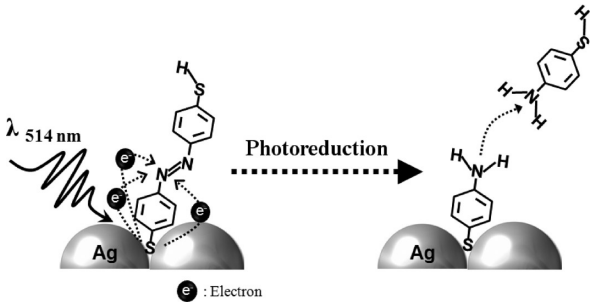

reduction of 4,4′-DMAB on Ag to 4-ABT suggested in this study. Although the work function of bulk silver is known to be ~4.3 eV, it has been observed by Fedurco et al. that the surface roughening of Ag results in a drastic increase of the photocurrent for the wavelength close to the surface plasmon frequency.[54] Thus, plasmonic nanostructures of noble metals (mainly silver and gold) have recently received significant attention for their potential future use in solar energy conversion.[55] Theoretically, it has also been suggested that excited plasmon states can interact through an electron-scattering process with the unpopulated adsorbate levels, leading to an electron-induced dissociation reaction on a photoexcited plasmonic metal.[56−59] On the other hand, water in ambient conditions has been claimed to act as a hydrogen source when 4-nitrobenzenethiol on Ag is converted to 4-ABT upon irradiation with an Ar^+ laser.[51] A similar assumption must be made in order to explain the photoinduced conversion of 4,4′-DMAB to 4-ABT on Ag. It shoud be noted that the photoconversion of 4,4′-DMAB on Ag to 4-ABT is a quite slow process even under the irradiation with a focused Ar^+ laser. At any rate, a novel experiment that clearly elucidates the mechanism of the photoinduced surface reaction, along with the origin of the hydrogen source, must be devised, and this will be one of our future research directions.

4. SUMMARY AND CONCLUSION

It has been claimed in the literature that 4-ABT on Ag can be converted to 4,4′-DMAB via a catalytic coupling reaction. The basis for this claim was the spectral similarity of 4-ABT and 4,4′-DMAB. We have argued against this view for a while, for several reasons. One reason was the observation that the appearance of the so-called b_2-type bands was a general phenomenon in the SERS of 4-ABT analogues, possibly including 4,4′-DMAB. Another specific reason was that 4,4′-DMAB on Ag seemed capable of being converted to 4-ABT not only by treatment with a 100 mM borohydride solution but also by exposure to a potential below −1.0 V, while the reverse reaction from 4-ABT to 4,4′-DMAB on Ag appeared to be insignificant electrochemically as well as photochemically. All together, developing a proper explanation of the origin of the b_2-type bands in the SERS of 4-ABT is a challenging step toward a deeper understanding of the SERS mechanisms. In this sense, it is of utmost importance to examine the SERS spectrum of 4,4′-DMAB itself more carefully and to compare its measured characteristics with those of 4-ABT. Thus, we carried out a SERS analysis of 4,4′-DMAB on Ag as a function of laser irradiation time. First, we found that when 514.5 nm radiation was used as the excitation source, the SERS spectral pattern of 4,4′-DMAB on Ag varied as a function of laser irradiation time, finally becoming the same as that of 4-ABT on Ag. This suggested the possibility of the photoconversion of 4,4′-DMAB on Ag to 4-ABT. To confirm this premise, we carried out an EDC coupling reaction and also attempted to grow a calcite crystal on 4,4′-DMAB on Ag. It was found that the EDC coupling reaction with 4-CBA proceeded readily on 4,4′-DMAB on Ag after it was exposed to 514.5 nm radiation but did not proceed without laser irradiation. Furthermore, the growth of a calcite crystal occurred readily on 4,4′-DMAB on Ag when it was similarly exposed to 514.5 nm radiation beforehand. On these grounds, we finally arrived at the conclusion that, first, the appearance of the so-called b_2-type bands in the SERS of 4-ABT must be due to the involvement of the chemical enhancement mechanism, not due to the formation of 4,4′-DMAB, and second, even under ambient conditions, 4,4′-DMAB on Ag could be converted to 4-ABT upon irradiation with 514.5 nm light, but not with 632.8 nm light. This observation is, in fact, opposite to claims previously made by several researchers.

■ ASSOCIATED CONTENT

Ⓢ Supporting Information

Vibrational assignments for the normal Raman and SERS spectra of 4,4′-DMAB and 4-ABT; FE-SEM images of calcite crystals grown on (a) 4-ABT and (b) 4,4′-DMAB on roughened Ag foil. This material is available free of charge via the Internet at http://pubs.acs.org.

■ AUTHOR INFORMATION

Corresponding Author

*Tel +82-2-8806651, Fax +82-2-8891568, e-mail kwankim@snu.ac.kr (K.K.); Tel +82-2-8200436, Fax +82-2-8244383, e-mail kshin@ssu.ac.kr (K.S.S.).

Notes

The authors declare no competing financial interest.

■ ACKNOWLEDGMENTS

This work was supported by a National Research Foundation (NRF) of Korea Grant funded by the Korean Government (MEST) (Grants 2007-0056334, 2012-0001352, 2012-0006225, and 2012008004).

■ REFERENCES

(1) Chang, R. K.; Furtak, T. E. *Surface Enhanced Raman Scattering*; Plenum Press: New York, 1982.

(2) Kneipp, K.; Wang, Y.; Kneipp, H.; Itzkan, I.; Dasari, R. R.; Feld, M. S. Population Pumping of Excited Vibrational States by

Spontaneous Surface-Enhanced Raman Scattering. *Phys. Rev. Lett.* **1996**, *76*, 2444−2447.
(3) Xu, H.; Bjerneld, E. J.; Käll, M.; Börjesson, L. Spectroscopy of Single Hemoglobin Molecules by Surface Enhanced Raman Scattering. *Phys. Rev. Lett.* **1999**, *83*, 4357−4360.
(4) Kleinman, S. L.; Ringe, E.; Valley, N.; Wustholz, K. L.; Phillips, E.; Scheidt, K. A.; Schatz, G. C.; Van Duyne, R. P. Single-Molecule Surface-Enhanced Raman Spectroscopy of Crystal Violet Isotopologues: Theory and Experiment. *J. Am. Chem. Soc.* **2011**, *133*, 4115−4122.
(5) Le Ru, E. C.; Grand, J.; Sow, I.; Somerville, W. R. C.; Etchegoin, P. G.; Treguer-Delapierre, M.; Charron, G.; Félidj, N.; Lévi, G.; Aubard, J. A Scheme for Detecting Every Single Target Molecule with Surface-Enhanced Raman Spectroscopy. *Nano Lett.* **2011**, *11*, 5013−5019.
(6) Moskovits, M. Surface-Enhanced Spectroscopy. *Rev. Mod. Phys.* **1985**, *57*, 783−826.
(7) Lombardi, J. R.; Birke, R. L. A Unified View of Surface-Enhanced Raman Scattering. *Acc. Chem. Res.* **2009**, *42*, 734−742.
(8) Nitzan, A.; Brus, L. E. Theoretical Model for Enhanced Photochemistry on Rough Surfaces. *J. Chem. Phys.* **1981**, *75*, 2205−2214.
(9) Goncher, G. M.; Harris, C. B. Enhanced Photofragmentation on A Silver Surface. *J. Chem. Phys.* **1982**, *77*, 3767−3768.
(10) Sandroff, C. J.; Herschbach, D. R. Surface-Enhanced Raman Study of Organic Sulfides Adsorbed on Silver: Facile Cleavage of Sulfur-Sulfur and Carbon-Sulfur Bonds. *J. Phys. Chem.* **1982**, *86*, 3277−3279.
(11) Goncher, G. M.; Parsons, C. A.; Harris, C. B. Photochemistry on Rough Metal Surfaces. *J. Phys. Chem.* **1984**, *88*, 4200−4209.
(12) Wolkow, R. A.; Moskovits, M. Enhanced Photochemistry on Silver Surfaces. *J. Chem. Phys.* **1987**, *87*, 5858−5869.
(13) Suh, J. S.; Jang, N. H.; Jeong, D. H.; Moskovits, M. Adsorbate Photochemistry on a Colloid Surface: Phthalazine on Silver. *J. Phys. Chem.* **1996**, *100*, 805−813.
(14) Lee, S. B.; Kim, K.; Kim, M. S. Electrochemical Reduction of Organic Sulfides Investigated by Raman Spectroscopy. *J. Phys. Chem.* **1992**, *96*, 9940−9943.
(15) Kim, K. L.; Lee, S. J.; Kim, K. Surface-Enhanced Raman Scattering of Benzyl Phenyl Sulfide in Ag Sol: Excitation-Wavelength Dependent Surface-Induced Photoreaction. *J. Phys. Chem. B* **2004**, *108*, 9216−9220.
(16) Fang, Y.; Li, Y.; Xu, H.; Sun, M. Ascertaining *p,p′*-Dimercaptoazobenzene Produced from *p*-Aminothiophenol by Selective Catalytic Coupling Reaction on Silver Nanoparticles. *Langmuir* **2010**, *26*, 7737−7746.
(17) Huang, Y. F.; Zhu, H. P.; Liu, G. K.; Wu, D. Y.; Ren, B.; Tian, Z. Q. When the Signal Is Not from the Original Molecule To Be Detected: Chemical Transformation of *para*-Aminothiophenol on Ag during the SERS Measurement. *J. Am. Chem. Soc.* **2010**, *132*, 9244−9246.
(18) Sun, M.; Xu, H. A Novel Application of Plasmonics: Plasmon-Driven Surface-Catalyzed Reactions. *Small* **2012**, *8*, 2777−2786.
(19) Wu, D.-Y.; Liu, X.-M.; Huang, Y.-F.; Ren, B.; Xu., X.; Tian., Z. Q. Surface Catalytic Coupling Reaction of *p*-Mercaptoaniline Linking to Silver Nanostructures Responsible for Abnormal SERS Enhancement: A DFT Study. *J. Phys. Chem. C* **2009**, *113*, 18212−18222.
(20) Sun, M.; Huang, Y.; Xia, L.; Chen, X.; Xu, H. The pH-Controlled Plasmon-Assisted Surface Photocatalysis Reaction of 4-Aminothiophenol to *p,p′*-Dimercaptoazobenzene on Au, Ag, and Cu Colloids. *J. Phys. Chem. C* **2011**, *115*, 9629−9636.
(21) Zong, S.; Wang, Z.; Yang, J.; Cui, Y. Intracellular pH Sensing Using *p*-Aminothiophenol Functionalized Gold Nanorods with Low Cytotoxicity. *Anal. Chem.* **2011**, *83*, 4178−4183.
(22) Hill, W.; Wehling, B. Potential- and pH-Dependent Surface-Enhanced Raman Scattering of *p*-Mercaptoaniline on Silver and Gold Substrates. *J. Phys. Chem.* **1993**, *97*, 9451−9455.
(23) Oldenburg, S. J.; Westcott, S. L.; Averitt, R. D.; J. Halas, N. J. Surface-enhanced Raman Scattering in The Near Infrared Using Metal Nanoshell Substrates. *J. Chem. Phys.* **1999**, *111*, 4729−4735.
(24) Li, J. F.; Huang, Y. G.; Zhi, Y. D.; Yang, L.; Li, S. B.; Zhou, X. S.; Fan, F. R.; Zhang, W.; Zhou, Z. Y.; Wu, D. Y.; Ren, B.; Wang, Z. L.; Tian, Z. Q. Shell-isolated Nanoparticle-enhanced Raman Spectroscopy. *Nature* **2010**, *464*, 392−395.
(25) Dendisová-Vyškovská, C.; Prokopec, V.; Člupek, M.; Matějka, P. Comparison of SERS Effectiveness of Copper Substrates Prepared by Different Methods: What Are The Values of Enhancement Factors ? *J. Raman Spectrosc.* **2012**, *43*, 181−186.
(26) Zhao, L. B.; Huang, R.; Huang, Y. F.; Wu, D. Y.; Ren, B.; Tian, Z. Q. Photon-driven Charge Transfer and Herzberg-Teller Vibronic Coupling Mechanism in Surface-Enhanced Raman Scattering of *p*-Aminothiophenol Adsorbed on Coinage Metal Surfaces: A Density Functional Theory Study. *J. Chem. Phys.* **2011**, *135*, 134707.
(27) Kim, K.; Shin, D.; Lee, H. B.; Shin, K. S. Surface-Enhanced Raman Scattering of 4-Aminobenzenethiol on Gold: The Concept of Threshold Energy in Charge Transfer Enhancement. *Chem. Commun.* **2011**, *47*, 2020−2022.
(28) Lombardi, J. R.; Birke, R. L. A Unified Approach to Surface-enhanced Raman Spectroscopy. *J. Phys. Chem. C* **2008**, *112*, 5605−5617.
(29) Osawa, M.; Matsuda, N.; Yoshii, K.; Uchida, I. Charge Transfer Resonance Raman Process in Surface-Enhanced Raman Scattering from *p*-Aminothiophenol Adsorbed on Silver: Herzberg-Teller Contribution. *J. Phys. Chem.* **1994**, *98*, 12702−12707.
(30) Zhou, Q.; Li, X.; Fan, Q.; Zhang, X.; Zheng, J. Charge Transfer between Metal Nanoparticles Interconnected with a Functionalized Molecule Probed by Surface-Enhanced Raman Spectroscopy. *Angew. Chem., Int. Ed.* **2006**, *45*, 3970−3973.
(31) Uetsuki, K.; Verma, P.; Yano, T.-A.; Saito, Y.; Ichimura, T.; Kawata, S. Experimental Identification of Chemical Effects in Surface Enhanced Raman Scattering of 4-Aminothiophenol. *J. Phys. Chem. C* **2010**, *114*, 7515−7520.
(32) Park, W.-H.; Kim, Z. H. Charge Transfer Enhancement in the SERS of a Single Molecule. *Nano Lett.* **2010**, *10*, 4040−4048.
(33) Kim, N. J. Physical Origins of Chemical Enhancement of Surface-Enhanced Raman Spectroscopy on a Gold Nanoparticle-Coated Polymer. *J. Phys. Chem. C* **2010**, *114*, 13979−13984.
(34) Ikeda, K.; Suzuki, S.; Uosaki, K. Crystal Face Dependent Chemical Effects in Surface-Enhanced Raman Scattering at Atomically Defined Gold Facets. *Nano Lett.* **2011**, *11*, 1716−1722.
(35) Wang, X.; Shi, W.; She, G.; Mu, L. Using Si and Ge Nanostructures as Substrates for Surface-Enhanced Raman Scattering Based on Photoinduced Charge Transfer Mechanism. *J. Am. Chem. Soc.* **2011**, *133*, 16518−16523.
(36) Ye, J.; Hutchison, J. A.; Uji-i, H.; Hofkens, J.; Lagae, L.; Maes, G.; Borghsa, G.; Van Dorpea, P. Excitation Wavelength Dependent Surface Enhanced Raman Scattering of 4-Aminothiophenol on Gold Nanorings. *Nanoscale* **2012**, *4*, 1606−1611.
(37) Kim, K.; Kim, K. L.; Shin, D.; Choi, J.-Y.; Shin, K. S. Surface-Enhanced Raman Scattering of 4-Aminobenzenethiol on Ag and Au: pH Dependence of b_2-Type Bands. *J. Phys. Chem. C* **2012**, *116*, 4774−4779.
(38) Kim, K.; Shin, D.; Choi, J.-Y.; Kim, K. L.; Shin, K. S. Surface-Enhanced Raman Scattering Characteristics of 4-Aminobenzenethiol Derivatives Adsorbed on Silver. *J. Phys. Chem. C* **2011**, *115*, 24960−24966.
(39) Kim, K.; Shin, D.; Kim, K. L.; Shin, K. S. Surface-Enhanced Raman Scattering of 4,4′-Dimercaptoazobenzene Trapped in Au Nanogaps. *Phys. Chem. Chem. Phys.* **2012**, *14*, 4095−4100.
(40) Kim, K.; Kim, K. L.; Lee, H. B.; Shin, K. S. Similarity and Dissimilarity in Surface-Enhanced Raman Scattering of 4-Aminobenzenethiol, 4,4′-Dimercaptoazobenzene, and 4,4′-Dimercaptohydrazobenzene on Ag. *J. Phys. Chem. C* **2012**, *116*, 11635−11642.
(41) Katz, E.; Itzhak, N.; Willner, I. Electron Transfer in Self-assembled Monolayers of *N*-Methyl-*N′*-carboxyalkyl-4,4′-bipyridinium Linked to Gold Electrodes. *Langmuir* **1993**, *9*, 1392−1396.

(42) Checkik, V.; Crooks, R. M.; Stirling, C. J. M. Reactions and Reactivity in Self-Assembled Monolayers. *Adv. Mater.* **2000**, *12*, 1161−1171.
(43) Han, S. W.; Lee, I.; Kim, K. Patterning of Organic Monolayers on Silver via Surface-Induced Photoreaction. *Langmuir* **2002**, *18*, 182−187.
(44) Albeck, S.; Aizenberg, J.; Addadi, L.; Weiner, S. Interactions of Various Skeletal Intracrystalline Components with Calcite Crystals. *J. Am. Chem. Soc.* **1993**, *115*, 11691−11697.
(45) Aizenberg, J.; Black, A.; Whitesides, G. M. Oriented Growth of Calcite Controlled by Self-Assembled Monolayers of Functionalized Alkanethiols Supported on Gold and Silver. *J. Am. Chem. Soc.* **1999**, *121*, 4500−4509.
(46) Lee, I.; Han, S. W.; Choi, H. J.; Kim, K. Nanoparticle-Directed Crystallization of Calcium Carbonate. *Adv. Mater.* **2001**, *13*, 1617−1620.
(47) Lee, P. C.; Meisel, D. Adsorption and Surface-enhanced Raman of Dyes on Silver and Gold Sols. *J. Phys. Chem.* **1982**, *86*, 3391−3395.
(48) Freeman, R. G.; Grabar, K. C.; Allison, K. J.; Bright, R. M.; Davis, J. A.; Guthrie, A. P.; Hommer, M. B.; Jackson, M. A.; Smith, P. C.; Walter, D. G.; Natan, M. J. Self-Assembled Metal Colloid Monolayers - An Approach to SERS Substrates. *Science* **1995**, *267*, 1629−1632.
(49) Lee, S. J.; Baik, J. M.; Moskovits, M. Polarization-Dependent Surface-Enhanced Raman Scattering from a Silver-Nanoparticle-Decorated Single Silver Nanowire. *Nano Lett.* **2008**, *8*, 3244−3247.
(50) Matsuda, N.; Sawaguchi, T.; Osawa, M.; Uchida, I. Surface-Assisted Photoinduced Reduction of *p*-Nitrothiophenol Self-Assembled Monolayer Adsorbed on a Smooth Silver Electrode. *Chem. Lett.* **1995**, 145−146.
(51) Kim, K.; Lee, Y. M.; Lee, H. B.; Park, Y.; Bae, T. Y.; Jung, Y. M.; Choi, C. H.; Shin, K. S. Visible Laser-Induced Photoreduction of Silver 4-Nitrobenzenethiolate Revealed by Raman Scattering Spectroscopy. *J. Raman Spectrosc.* **2010**, *41*, 187−192.
(52) Han, S. W.; Han, H. S.; Kim, K. Infrared and Raman Spectra of 4-Cyanobenzoic Acid on Powdered Silver. *Vib. Spectrosc.* **1999**, *21*, 133−142.
(53) Bahng, M. K.; Cho, N. J.; Park, J. S.; Kim, K. Interaction of Indolicidin with Model Lipid Bilayers: FTIR-ATR Spectroscopic Study. *Langmuir* **1998**, *14*, 463−470.
(54) Fedurco, M.; Shklover, V.; Augustynski, J. Effect of Halide Ion Adsorption upon Plasmon-Mediated Photoelectron Emission at the Silver/Solution Interface. *J. Phys. Chem. B* **1997**, *101*, 5158−5165.
(55) Christopher, P.; Xin, H.; Linic, S. Visible Light Enhanced Catalytic Oxidation Reactions on Plasmonic Ag Nanostructures. *Nat. Chem.* **2011**, *3*, 467−472.
(56) Buntin, S. A.; Richter, L. J.; Cavanagh, R. R.; King, D. S. Optically Driven Surface Reactions: Evidence for the Role of Hot Electrons. *Phys. Rev. Lett.* **1998**, *61*, 1321−1324.
(57) Brus, L. Noble Metal Nanocrystals: Plasmon Electron Transfer Photochemistry and Single-Molecule Raman Spectroscopy. *Acc. Chem. Res.* **2008**, *41*, 1742−1749.
(58) Olsen, T.; Gavnholt, J.; Schiotz, J. Hot-Electron-Mediated Desorption Rates Calculated from Excited-State Potential Energy Surfaces. *Phys. Rev. B* **2009**, *79*, 035403.
(59) Adleman, J. R.; Boyd, D. A.; Goodwin, D. G.; Psaltis, D. Heterogenous Catalysis Mediated by Plasmon Heating. *Nano Lett.* **2009**, *9*, 4417−4423.